The Resonant Cylindrical Dielectric Cavity Antenna

STUART A. LONG, SENIOR MEMBER, IEEE, MARK W. McALLISTER, AND LIANG C. SHEN, SENIOR MEMBER, IEEE

Abstract—**An experimental investigation of the radiation and circuit properties of a resonant cylindrical dielectric cavity antenna has been undertaken. The radiation patterns and input impedance have been measured for structures of various geometrical aspect ratios, dielectric constants, and sizes of coaxial feed probes. A simple theory utilizing the magnetic wall boundary condition is shown to correlate well with measured results for radiation patterns and resonant frequencies.**

I. INTRODUCTION

IN RECENT YEARS the frequency range of interest for many systems has gradually progressed upward. For applications today, frequencies beyond the usual microwave band and in the millimeter and near millimeter region (100-300 GHz) are often required. Most of the antennas that are in current use in the microwave band cannot be simply scaled up in frequency. Conduction losses in any metal portion of the radiating structure do not remain constant after scaling, and, as a result, these losses may become too great for systems requiring efficient operation. For other applications, excessive reduction in size may prohibit economical fabrication.

A novel structure which seemingly has the possibility of radiating efficiently in this frequency range is the resonant cylindrical dielectric cavity antenna. Previously dielectric cylinders of very high permittivity (relative dielectric constants of the order of 100-300) have been used as resonant cavities [1]-[6]. Theoretical studies of the dielectric cavity have been previously reported by Van Bladel [7], [8]. In each case the emphasis of the investigation has been on the structure as an energy storage device, but since the cavity is not enclosed by metallic walls, electromagnetic fields do exist beyond the geometrical boundary of the cavity. Little or no work has been devoted to this structure as a radiator, nor has a complete investigation of the external fields been made. With the use of lower dielectric constant materials ($5 \leqslant \epsilon_r \leqslant 20$), and proper choices of the dimensions of the cylinder, these radiation fields can be enhanced.

Experimental measurements have been made on several dielectric cylinders with varying geometrical aspect ratios, dielectric constants, and feed probe lengths. This work indicates that such an antenna can be designed to provide reasonably efficient radiation in the direction normal to the ground plane of the antenna. A simple theory utilizing the magnetic wall boundary condition is shown to correlate well with measured results for radiation patterns and resonant frequencies.

This type of radiator seemingly has several features which may be exploited over previously developed millimeter leaky wave antennas. Being a resonant structure, higher efficiencies may be expected, provided that suitable materials with low dielectric loss characteristics are utilized. Control of the radiated fields may also prove to be simpler with the main lobe of radiation remaining normal to the ground plane of the structure with variations in geometry and frequency. In addition, circular polarization can probably be obtained by slight changes in geometry in much the same fashion as has been previously accomplished with printed-circuit antennas [9].

Even though the emphasis of this paper is on the experimental verification of the utility of this radiating structure, the approximate theoretical analysis is presented first. The simple magnetic wall model cannot be rigorously applied for the values of dielectric constants considered. However, this method of attacking the theoretical problem provides a first order solution which is seen to provide reasonably accurate predictions for the radiation patterns and resonant frequencies. A more complicated model may be needed for other properties, such as the near field and the overall impedance, which are more sensitive to the exact field distributions.

Manuscript received April 5, 1982; revised September 9, 1982. This work was supported in part by the U.S. Army Research Office through the Laboratory Research Cooperative Program and under Contract DAAG29-82-K-0074.

The authors are with the Department of Electrical Engineering, Cullen College of Engineering, University of Houston, Houston, TX 77004.

II. THEORETICAL DERIVATIONS

A. Boundary Value Problem and Resonant Frequencies

The geometry of the problem is shown in Fig. 1 using standard cylindrical coordinates. The feed probe is temporarily ignored, i.e., the cylinder is considered uniform. Image theory can be immediately applied and the ground plane can be replaced by an imaged portion of the cylinder extending to $z = -d$; the isolated cylinder is now analyzed with an implied boundary condition of zero E_ρ and E_ϕ at $z = 0$.

An approximate solution for the fields inside such a cylinder can be obtained by assuming that the surfaces are perfect magnetic conductors. This technique has been previously justified [1]. For such a cavity, wave functions transverse electric (TE) and transverse magnetic (TM) to z may be postulated

$$\psi_{\mathrm{TE}_{npm}} = J_n\left(\frac{X_{np}}{a}\rho\right)\begin{Bmatrix}\sin n\phi\\ \cos n\phi\end{Bmatrix}\sin\left[\frac{(2m+1)\pi}{2d}\right] \tag{1}$$

$$\psi_{\mathrm{TM}_{npm}} = J_n\left(\frac{X'_{np}}{a}\rho\right)\begin{Bmatrix}\sin n\phi\\ \cos n\phi\end{Bmatrix}\cos\frac{(2m+1)\pi z}{2d} \tag{2}$$

where J_n is the Bessel function of the first kind,

$$J_n(X_{np}) = 0, J'_n(X'_{np}) = 0,$$

$$n = 1, 2, 3\cdots, p = 1, 2, 3, \cdots, \quad m = 0, 1, 2\cdots.$$

The separation equation $k_\rho^2 + k_z^2 = k^2 = \omega^2\mu\epsilon$ leads to an expression for the resonant frequency of the *npm* mode.

$$f_{npm} = \frac{1}{2\pi a\sqrt{\mu\epsilon}}\sqrt{\begin{Bmatrix}X_{np}^2\\ X_{np}'^2\end{Bmatrix} + \left[\frac{\pi a}{2d}(2m+1)\right]^2}. \tag{3}$$

The dominant mode is the one which has the lowest resonant fre-

0018-926X/83/0500-0406$01.00

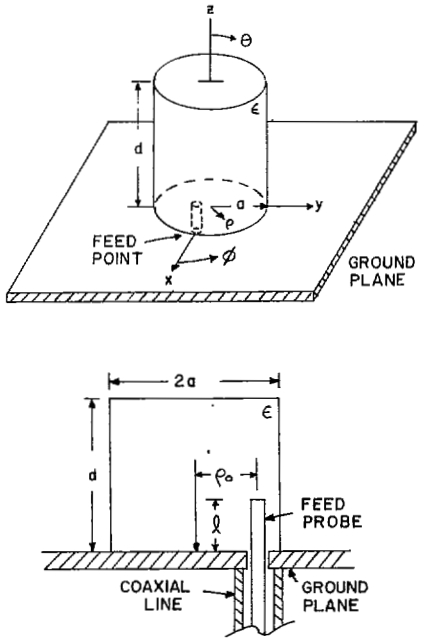

Fig. 1. Antenna geometry and feed configuration.

quency. This occurs for $m = 0, n = 1, p = 1$: $X'_{11} = 1.841$.

$$f_{\mathrm{dom}} = \frac{1}{2\pi a\sqrt{\mu\epsilon}}\sqrt{X'^2_{11} + \left(\frac{\pi a}{2d}\right)^2}. \tag{4}$$

B. Equivalent Magnetic Surface Currents for the Dominant Mode

The wave function of the dominant mode is

$$\psi_{\mathrm{TM}_{110}} = \psi = J_1\left(\frac{X'_{11}\rho}{a}\right)\cos\phi\cos\frac{z\pi}{2d}. \tag{5}$$

The cos ϕ term, rather than sin ϕ, survives due to the feed position at $\phi = 0$. In anticipation of calculating the far-field patterns, tangential electric fields on the surface are determined using

$$E_\phi = \frac{1}{j\omega\epsilon\rho}\frac{\partial^2\psi}{\partial\phi\partial z}, \quad E_z = \frac{1}{j\omega\epsilon}\left(\frac{\partial^2}{\partial z^2} + k^2\right)\psi,$$

$$E_\rho = \frac{1}{j\omega\epsilon}\frac{\partial^2\psi}{\partial\rho\partial z}. \tag{6}$$

Applying $\vec{M} = \vec{E} \times \hat{n}$, where $\hat{n}$ is a unit normal pointing out of the dielectric, the following equivalent currents are found (primed coordinates are used to indicate the source).

Sides:

$$M_{z'} = \frac{\pi}{2j\omega\epsilon ad}J_1(X'_{11})\sin\phi'\sin\frac{\pi z'}{2d} \tag{7}$$

and

$$M_{\phi'} = \frac{1}{j\omega\epsilon}\left(\frac{X'_{11}}{a}\right)^2 J_1(X'_{11})\cos\phi'\cos\frac{\pi z'}{2d}. \tag{8}$$

Top-bottom:

$$M_{\phi'} = \frac{\pi X'_{11}}{j2\omega\epsilon ad}J'_1\left(\frac{X'_{11}\rho'}{a}\right)\cos\phi' \tag{9}$$

and

$$M_{\rho'} = \frac{\pi}{j2\omega\epsilon d\rho'}J_1\left(\frac{X'_{11}\rho'}{a}\right)\sin\phi'. \tag{10}$$

C. Calculation of Far-Field Patterns

The above currents are considered the sources for the far-field radiation. Since the radiation fields will be expressed in spherical coordinates (r, θ, ϕ), the source currents are transformed:

$$M_\theta = M_{\rho'}\cos\theta\cos(\phi - \phi') + M_{\phi'}\cos\theta\sin(\phi - \phi') - M_{z'}\sin\theta \tag{11}$$

$$M_\phi = -M_{\rho'}\sin(\phi - \phi') + M_{\phi'}\cos(\phi - \phi'). \tag{12}$$

Electric vector potentials are then calculated:

$$F_\theta = \frac{e^{-jk_0 r}}{4\pi r}\iiint M_\theta e^{jk_0[\rho'\sin\theta\cos(\phi-\phi')+z'\cos\theta]}\rho'\,d\rho'\,d\phi'\,dz \tag{13}$$

$$F_\phi = \frac{e^{-jk_0 r}}{4\pi r}\iiint M_\phi e^{jk_0[\rho'\sin\theta\cos(\phi-\phi')+z'\cos\theta]}\rho'\,d\rho'\,d\phi'\,dz, \tag{14}$$

where $k_0 = \omega\sqrt{\mu_0\epsilon_0}$ (the free space wavenumber).

Summing the individual contributions to M_θ and M_ϕ, and integrating results in

$$F_\theta = C_1\{I_2 - I_1 - 0.5k_\rho(I_3 + I_4 - I_5 - I_6) + 1.16k_0\sin\theta J_1(k_0 a\sin\theta)D_1 - 0.581k_\rho^2 a \cdot [J_0(k_0 a\sin\theta) + J_2(k_0 a\sin\theta)]D_1\} \tag{15}$$

$$F_\phi = C_2\{-I_1 - I_2 - 0.5k_\rho(I_3 - I_4 - I_5 + I_6) - 0.581k_\rho^2 a[J_0(k_0 a\sin\theta) - J_2(k_0 a\sin\theta)]D_1\} \tag{16}$$

where

$$C_1 = \frac{\pi^2}{j\omega\epsilon d}\frac{1}{4\pi r}\sin\phi\cos(k_0 d\cos\theta)\cos\theta \tag{17}$$

$$C_2 = \frac{\pi^2}{j\omega\epsilon d}\frac{1}{4\pi r}\cos\phi\cos(k_0 d\cos\theta) \tag{18}$$

$$D_1 = \left[\frac{\pi^2}{4d^2} - k_0^2\cos^2\theta\right]^{-1} \tag{19}$$

$$k_\rho = \frac{X'_{11}}{a} = \frac{1.841}{a} \tag{20}$$

$$I_1 = \int_0^a J_1(k_\rho\rho')J_0(k_0\rho'\sin\theta)\,d\rho' \tag{21}$$

$$I_2 = \int_0^a J_1(k_\rho\rho')J_2(k_0\rho'\sin\theta)\,d\rho' \tag{22}$$

$$I_3 = \int_0^a J_0(k_\rho\rho')J_0(k_0\rho'\sin\theta)\rho'\,d\rho' \tag{23}$$

$$I_4 = \int_0^a J_0(k_\rho\rho')J_2(k_0\rho'\sin\theta)\rho'\,d\rho' \tag{24}$$

$$I_5 = \int_0^a J_2(k_\rho \rho') J_0(k_0 \rho' \sin\theta) \rho' \, d\rho' \tag{25}$$

$$I_6 = \int_0^a J_2(k_\rho \rho') J_2(k_0 \rho' \sin\theta) \rho' \, d\rho'. \tag{26}$$

For the permittivities and aspect ratios under consideration ($a/d \leqslant 2$, $\epsilon_r \geqslant 5$), the term $k_0 a$ will always be less than two; this allows polynomial approximations for the above Bessel functions to be used, and the integrals are easily evaluated numerically.

In the far-field region, the electric fields are proportional to the vector potential $\vec{F}$: $E_\theta \alpha F_\phi$, and $E_\phi \alpha F_\theta$. The radiation patterns are thus found as a function of the antenna parameters.

III. THEORETICAL CALCULATIONS

The resonant frequencies as given by (3) are shown for four selected a/d ratios in Table I. The next lowest order mode after the dominant TM_{110} can either be the TM_{111} (as in the case of small a/d ratios) or the TE_{010} (for large a/d). The higher order resonances are shown for each cylinder with $\epsilon_r = 8.9$. Table II gives the resonant frequencies for several different dielectric constants for the case of $a/d = 0.5$ and $a = 0.0127$ m (a diameter of 1 in).

To illustrate the dependence of the far fields on the parameters of the antenna, several radiation patterns can be plotted. In each case the fields are shown in two principal planes. The radiated field is polarized so that it is parallel to a plane formed by a radial line from the center of base of the cylinder to the feed point and a line perpendicular to the ground plane. Since the feed is located at the $\phi = 0°$, $\rho = a$, $z = 0$ position as shown previously in Fig. 1, a graph showing E_θ versus θ for $\phi = 0, 180°$ is one principal pattern of interest. The second is that for E_ϕ at $\phi = 90°$, 270°. The major features of the radiation properties of the antenna are shown in these two patterns.

The dependence of E_θ on the shape of the cylinder (the ratio a/d) is shown in Fig. 2(a). The field is essentially omnidirectional for cylinders with larger a/d ratios. For smaller a/d ratios a null begins to develop along the direction normal to the plane of the radiator. E_ϕ in the $\phi = 90°$ plane is also shown in Fig. 2(b). A 3 dB beamwidth of 85° or greater is characteristic of the values obtained. As a/d is reduced, a dip also begins to appear in the $\theta = 0°$ direction.

IV. EXPERIMENTAL MEASUREMENTS

A. Radiation Patterns

Various dielectric materials were acquired, and cylinders were machined with different a/d ratios. One set of cylinders with various a/d ratios (see data in Table I) was made from material with $\epsilon_r = 8.9$ and mounted on a circular ground plane of diameter 7.6 cm (3 in). The sizes were chosen so that the dominant mode resonance would be near 10 GHz. Each radiator was fed by the inner conductor of a coaxial line which extended through the ground plane a distance of $l = 0.38$ cm into a hole located near the edge of the cylinder (see Fig. 1). A second set of cylinders all with $a/d = 0.5$ and $a = 0.0127$m (diameter is 1 in) was fabricated out of three different materials with $\epsilon_r = 15.2$, 6.6, and 4.5. These radiators were mounted on a 61 cm (24 in) square ground plane, were fed in a similar fashion with a longer probe of $l = 1.45$ cm, and had predicted resonances between 2.0-3.5 GHz. Far-field radiation patterns were measured in the two principal planes with the overall field linearly polarized in the $\hat{x}$ direction at $\theta = 0°$.

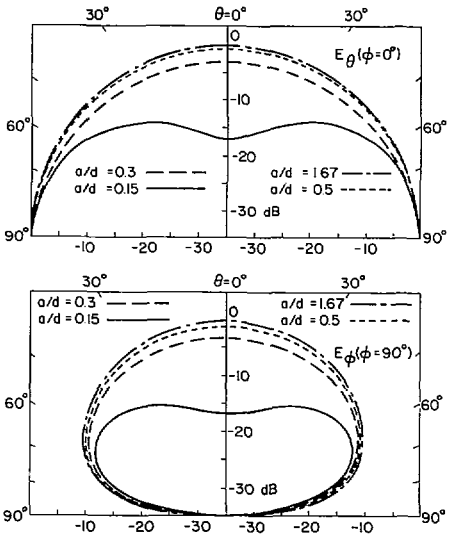

Fig. 2. Theoretical radiation patterns for various a/d ratios.

TABLE I
RESONANT FREQUENCIES (IN GHz) FOR VARIOUS a/d RATIOS ($\epsilon_r = 8.9$)

Mode	m =	0	1	2
TM_{11m}		10.13	12.38	15.95
TE_{01m}		13.07	14.88	17.97
TM_{21m}		16.48	17.96	20.58

$a/d = 0.3$, $a = 0.3$ cm; $d = 1.0$ cm, $\epsilon_r = 8.9$.

Mode	m =	0	1	2
TM_{11m}		10.67	15.95	23.14
TE_{01m}		13.49	17.97	24.57
TM_{21m}		16.82	20.58	26.54

$a/d = 0.5$, $a = 0.3$ cm; $d = 0.6$ cm, $\epsilon_r = 8.9$.

Mode	m =	0	1	2
TM_{11m}		10.24	25.82	42.32
TE_{01m}		11.38	26.29	42.60
TM_{21m}		12.48	26.98	43.03

$a/d = 1.67$, $a = 0.5$ cm; $d = 0.3$ cm, $\epsilon_r = 8.9$.

Mode	m =	0	1	2
TM_{11m}		9.90	10.53	11.66
TE_{01m}		12.89	13.38	14.29
TM_{21m}		16.35	16.72	17.46

$a/d = 0.15$, $a = 0.3$ cm; $d = 2.0$ cm; $\epsilon_r = 8.9$.

TABLE II
RESONANT FREQUENCIES (IN GHz) FOR VARIOUS DIELECTRIC CONSTANTS ($a = 0.0127$ m, $a/d = 0.5$)

Mode	$\epsilon_r = 15.2$	8.9	6.6	4.5
TM_{110}	1.93	2.52	2.93	3.55
TE_{010}	2.44	3.19	3.70	4.49
TM_{111}	2.89	3.77	4.38	5.30
TM_{210}	3.04	3.97	4.62	5.59
TE_{011}	3.25	4.24	4.93	5.97
TM_{211}	3.72	4.86	5.65	6.84

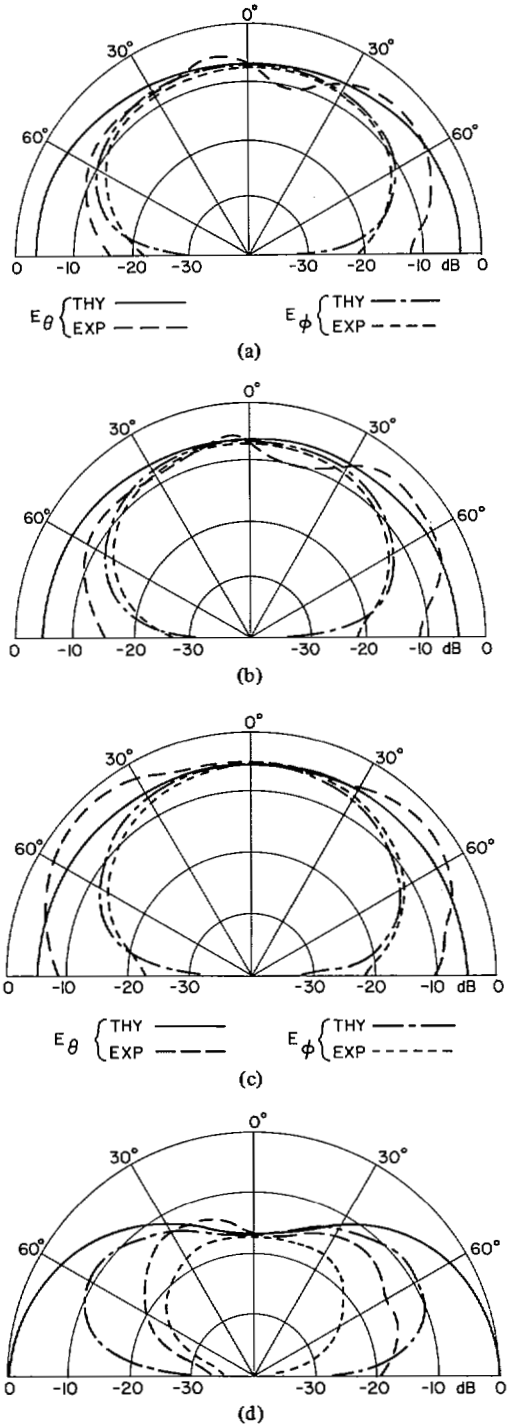

Fig. 3. Theoretical and experimental fields. (a) a/d = 0.3. (b) a/d = 0.5. (c) a/d = 1.67. (d) a/d = 0.15.

Fig. 3 illustrates the measured field patterns for the four cylinders with different values of radius-to-height ratios a/d along with the theoretically predicted fields of the past section. Reasonable agreement is found for the first three radiators. In each case the measured values of E_θ show a broad, almost omnidirectional pattern with some scalloping and a roll-off near $\theta = 90°$ (both a result of the finite ground plane used for the experimental measurements). As the a/d ratio is allowed to decrease to 0.15 for the last sample the experimental E_θ has only a dip of about 5 dB at $\theta = 0°$ as opposed to a 10 dB dip in the theory. The experimental E_ϕ shows no dip at all as compared to a theoretical one of 8 dB. It should be noted that in each case that the theoretical fields were normalized by setting the theoretical E_θ equal to the experimental value at $\theta = 0°$. All other fields shown (both E_θ and E_ϕ) are, therefore, relative to that value. When compared to a standard gain horn, a representative pattern ($a/d = 0.3$) showed an overall gain of approximately -1 dB below isotropic.

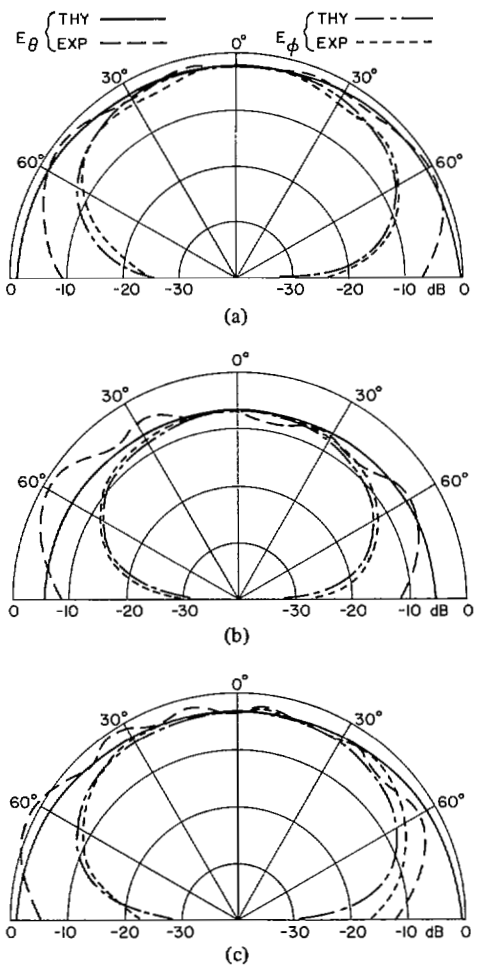

Fig. 4. Theoretical and experimental fields. (a) ϵ_r = 15.2. (b) ϵ_r = 6.6. (c) ϵ_r = 4.5.

Fig. 4 shows the measured field patterns for the identically sized cylinders with different values of dielectric constant. Again the normalized theoretical fields are shown for comparison. Good agreement is seen again for both planes except near $\theta = 90°$ due to the finite ground plane.

B. Impedance Measurements

To determine the effects of the shape of the cylinder on the circuit characteristics of the radiator, four cylinders were fabricated with various radius-to-height ratios. Each antenna was made from the same dielectric material with $\epsilon_r = 8.9$ and fed near its edge by the center conductor of a coaxial line which extended $l = 0.38$ cm into the cylinder. The sizes were chosen so that the theoretical value of the lowest resonant frequency would be between 9.9 and 10.7 GHz. The dimensions and first resonance are shown in Table III.

The input impedance of each cylinder was measured and its magnitude and its real and imaginary parts are shown as a function of frequency in Fig. 5. Since several closely spaced modes are excited, the usual pure resonance curves are distorted somewhat. In addition, an inductive shift causes the maximum of the real part of the impedance and the zero of the imaginary part

TABLE III
ANTENNA DESIGN PARAMETERS

Sample Number	a (cm)	d (cm)	a/d	Frequency (GHz)
1	0.3	1.0	0.3	10.13
2	0.3	0.6	0.5	10.67
3	0.5	0.3	1.67	10.24
4	0.3	2.0	0.15	9.90

not to occur at exactly the same frequency. When comparing with the theoretical resonant frequencies, the point where the real part is a maximum was chosen as the experimental value. For sample 1 with $a/d = 0.3$, the first resonance occurs just above 10 GHz very near the theoretical value of 10.13 GHz. The impedance measured for sample 2 ($a/d = 0.5$) shows a resonance near 10.5 GHz as compared to the theoretical value of 10.67 GHz (an error of ~1.6 percent). Similar behavior is seen for sample 3 ($a/d = 1.67$). The resonance near 10.5 GHz is above that of the predicted 10.24 GHz (an error of ~2.5 percent). In the case of sample 4 the first two modes are seen to be very close to each other in frequency, corresponding to the predicted values of 9.90 and 10.52 GHz for the TM_{110} and TM_{111} modes. The first mode does seem to appear near 10 GHz however.

To ascertain the effect of the dielectric constant of the material used for the cylinder, more cylinders were fabricated with $a/d = 0.5$ from materials with $\epsilon_r = 15.2$, 8.9, 6.6, and 4.5, respectively. In this instance, however, the raw stock was in the form of cylindrical rods of approximately 1-in diameter ($a = 1.283$ cm). This material was cut so that $a/d = 0.5$ and the resulting cylinders were fed by probes with $l = 1.54$ cm. Owing to their larger size, the resonant frequencies were reduced into the S-band region (2-4 GHz).

The resulting real and imaginary parts of the impedance are shown as a function of frequency in Fig. 6. Once again reasonable agreement is found between theory and experiment for the first resonant frequency. For $\epsilon_r = 15.2$ the resonance near 2.0 GHz is about 3.6 percent above the predicted 1.931 GHz. For $\epsilon_r = 8.9$ the experimental value of 2.62 GHz is above the theoretical value of 2.52 GHz by four percent. The predicted value of 2.93 GHz is within one percent of the measured 2.95 GHz for $\epsilon_r = 6.6$, while for the case of $\epsilon_r = 4.5$ the experimental value of 3.45 GHz is about three percent from the theoretical 3.55 GHz.

Previous work in analyzing similar structures with much higher dielectric constants using the magnetic wall model typically have errors of approximately five to 10 percent in the prediction of the resonant frequencies. These are almost always TE modes, however, and in our case the mode of interest is a TM one. In Yee's work [1], using materials with $\epsilon_r = 100$, resonances were found to occur at frequencies corresponding to errors of less than one percent. Thus for our lower dielectric constant materials errors of two to five percent appear to be reasonable.

C. Impedance Matching

In all previous measurements the feed was located at a point near the edge of the cylinder. Since the z-directed electric field has a radial variation like $J_1(1.841\rho/a)$, it should be possible to change the impedance by shifting the position of the feed away from the edge. This technique has been previously exploited as an impedance matching technique in the case of the circular-disk

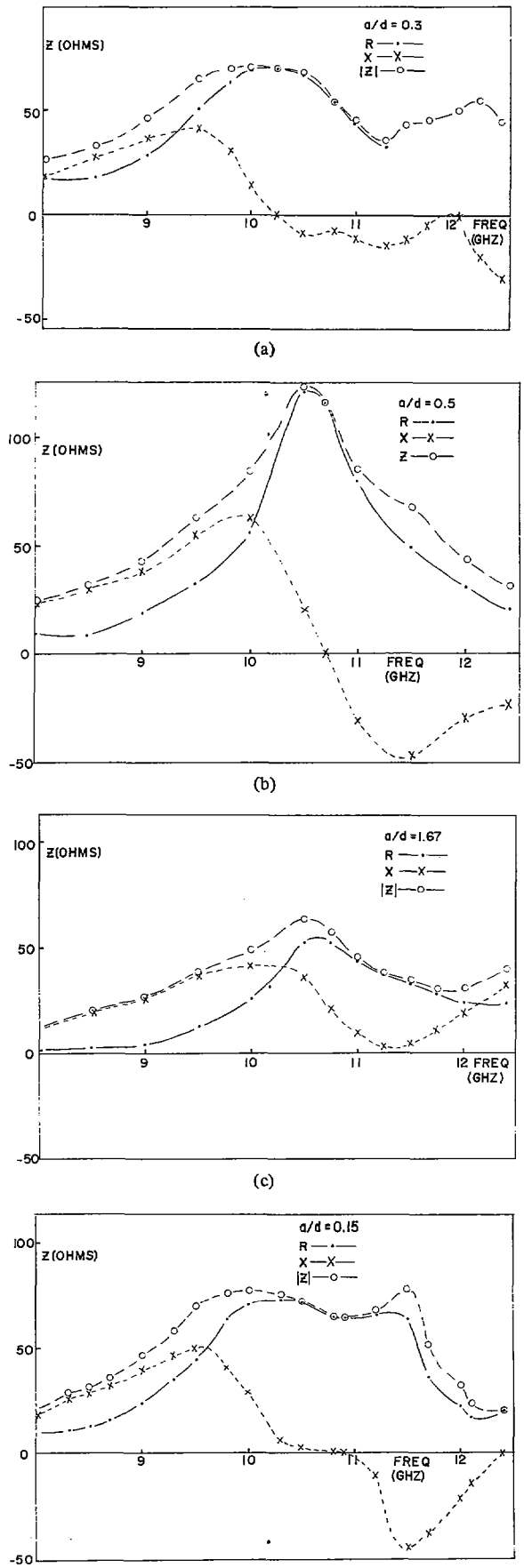

Fig. 5. Measured impedance versus frequency for various a/d ratios; $\epsilon_r = 8.9$. (a) $a/d = 0.3$. (b) $a/d = 0.5$. (c) $a/d = 1.67$. (d) $a/d = 0.15$.

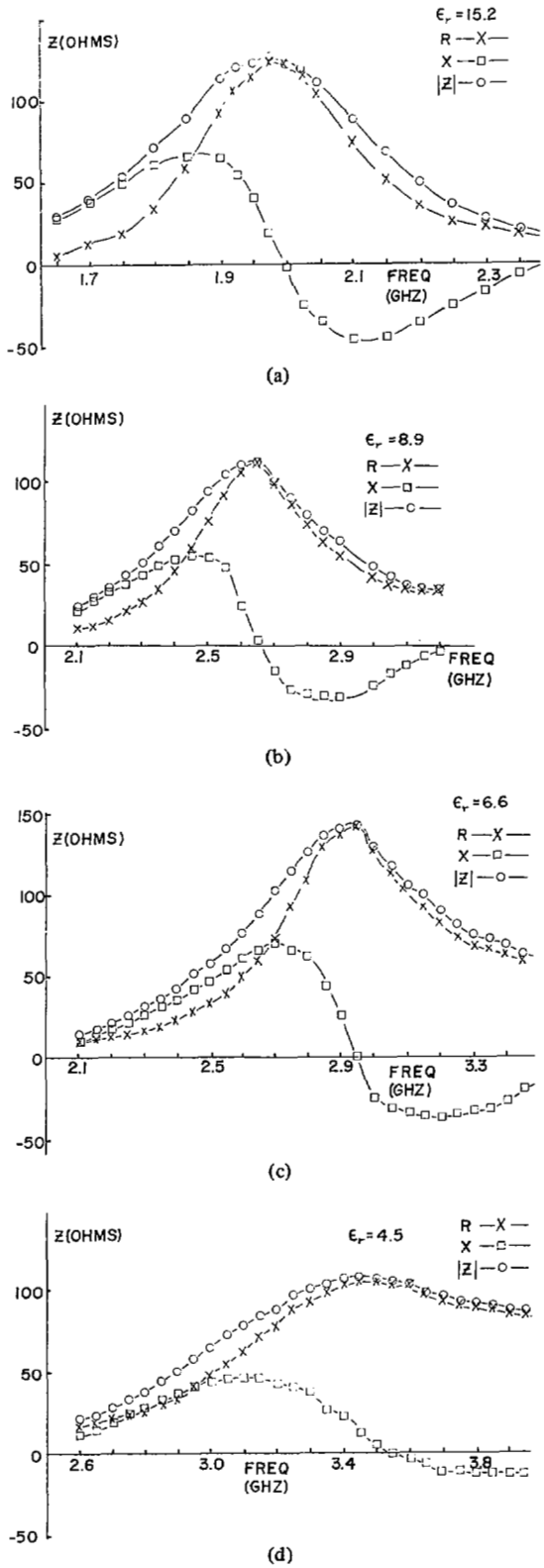

Fig. 6. Measured impedance versus frequency for various values of ϵ_r; $a/d = 0.5$. (a) $\epsilon_r = 15.2$. (b) $\epsilon_r = 8.9$. (c) $\epsilon_r = 6.6$, (d) $\epsilon_r = 4.5$.

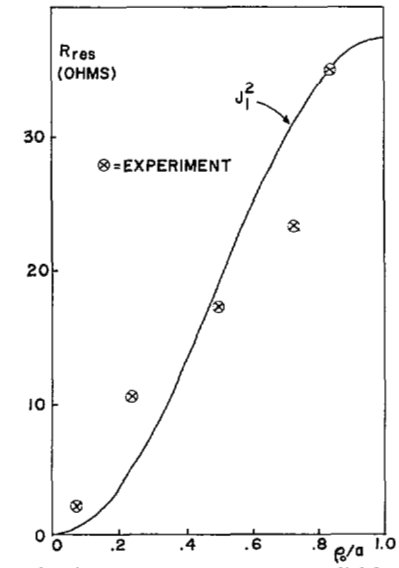

Fig. 7. Measured resistance at resonance versus radial feed point position.

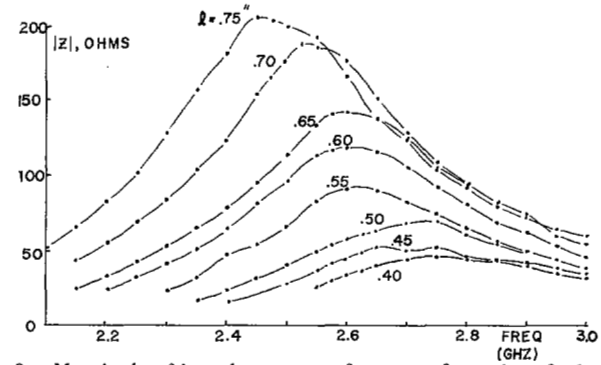

Fig. 8. Magnitude of impedance versus frequency for various feed probe lengths (in inches): $\epsilon_r = 8.9$; $a/d = 0.5$; $a = 0.0127$ m.

printed-circuit antenna [11]. As previously derived [11], the resistance at resonance resulting from the given E_z dependence on radial position gives a theoretical variation in impedance proportional to $J_1^2(k_\rho \rho_0)$ where ρ_0 is the radial coordinate of the feed position. The resistance at resonance was measured at five different feed positions for a radiator with $\epsilon_r = 15.2$ and $l = 0.38$ cm and the theory was normalized at the outermost one ($\rho_0/a = 0.83$). This theoretical curve is shown in Fig. 7 along with the five experimental values. Even though fluctuations are seen, the general behavior is verified at least in a qualitative sense.

Another matching technique which is apparent from the lower values of resistance at resonance seen in Fig. 7 is the variation in feed probe length. Impedance measurements were taken for a cylinder with $\epsilon_r = 8.9$ ($a/d = 0.5$, $a = 0.0127$ m) for feed probe lengths varying from $l = 0.40$ to 0.75 in (1.0 to 1.9 cm). The resulting magnitudes of the impedances are shown in Fig. 8 and the ability to control the resistance at resonance by varying the feed length can be seen.

It should be noted that the measured impedance behavior is really a combination of two effects—one due to the resonance associated with the dielectric cylinder and the other from the feed probe itself. The length of the feed seems to affect mainly the magnitude of the impedance at resonance while the size of the cylinder is most important in determining the resonant frequency. Any meaningful attempt to predict the actual impedance behavior theoretically must include both of these effects.

V. CONCLUSION

An introductory experimental investigation of the resonant cylindrical dielectric cavity antenna has been made. This antenna was shown to be capable of providing efficient radiation in the direction normal to its ground plane while retaining many desirable features necessary for future applications in the millimeter wave frequency region. The radiation and circuit properties were measured as a function of the physical parameters of the cylinder and reasonable correlation was found when compared with a simple theory based on a magnetic wall boundary condition.

ACKNOWLEDGMENT

The authors would like to acknowledge the aid of Fred Farrar and the other members of the microwave branch at the Harry Diamond Laboratories, Adelphi, MD, for their aid in the experimental portion of this work during the summer of 1981.

REFERENCES

[1] H. Y. Yee, "Natural resonant frequencies of microwave dielectric resonators," *IEEE Trans. Microwave Theory Tech.*, vol. MTT-13, p. 256, Mar. 1965.

[2] K. K. Chow, "On the solution and field pattern of cylindrical dielectric resonators," *IEEE Trans. Microwave Theory Tech.*, vol. MTT-14, pp. 439, Sept. 1966.

[3] S. B. Cohn, "Microwave band-pass filters containing high-Q dielectric resonators," *IEEE Trans. Microwave Theory Tech.*, vol. MTT-16, pp. 218–227, Apr. 1968.

[4] T. Itoh and R. Rudokas, "New method for computing the resonant frequencies of dielectric resonators," *IEEE Trans. Microwave Theory Tech.*, vol. MTT-25, pp. 52–55, Jan. 1977.

[5] C. Chang and T. Itoh, "Resonant characteristics of dielectric resonators for millimeter-wave integrated circuits," *Archiv für Elektronik and Übertragungstechnik*, vol. 33, pp. 141–144, Apr. 1979.

[6] P. Guillon and Y. Garault, "Accurate resonant frequencies of dielectric resonators," *IEEE Trans. Microwave Theory Tech.*, MTT-25, pp. 916–922, Nov. 1977.

[7] J. Van Bladel, "On the resonances of a dielectric resonator of very high permittivity," *IEEE Trans. Microwave Theory Tech.*, vol. MTT-23, pp. 199–208, Feb. 1975.

[8] ——, "The excitation of dielectric resonators of very high permittivity," *IEEE Trans. Microwave Theory Tech.*, vol. MTT-23, pp. 208–217, Feb. 1975.

[9] S. A. Long, L. C. Shen, D. H. Schaubert, and F. Farrar, "An experimental study of the circular polarized elliptical printed-circuit antenna," *IEEE Trans. Antennas Propagat.*, vol. AP-29, pp. 95–99, Jan. 1981.

[10] M. Abramowitz and I. Stegun, Eds., *Handbook of Mathematical Functions*, Washington, DC: Nat. Bur. Stand., 1968.

[11] S. Long, L. Shen, M. Walton, and M. Allerding, "Impedance of a circular-disc printed-circuit antenna," *Electron. Lett.*, vol. 14, no. 21, pp. 684–686, Oct. 12, 1978.

Stuart A. Long (S'65–S'72–M'74–SM'80), for a photograph and biography please see page 98 of the January 1981 issue of this TRANSACTIONS.

Mark W. McAllister, for a photograph and biography please see page 1200 of the November 1982 issue of this TRANSACTIONS.

Liang C. Shen (S'65–M'67–SM'77), for a photograph and biography please see page 94 of the January 1981 issue of this TRANSACTIONS.